Journal of Energy Storage 68 (2023) 107670

Contents lists available at ScienceDirect

Journal of Energy Storage

journal homepage: www.elsevier.com/locate/est

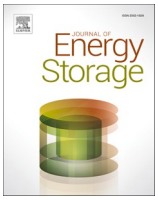

Research papers

Study of the influence of the type of pores present in the electrodes on the behaviour of a SWAGELOK-type supercapacitor

Jesús M. Rodríguez-Rego [a], Laura Mendoza-Cerezo [a], Alfonso C. Marcos-Romero [b], Juan P. Carrasco-Amador [b], A. Macías-García [a,*]

[a] Departamento de Ingeniería Mecánica, Energética y de Materiales, Escuela Técnica Superior de Ingenieros Industriales, Universidad de Extremadura, Avda. de Elvas s/n, 06006 Badajoz, España

[b] Departamento de Expresión Gráfica, Escuela Técnica Superior de Ingenieros Industriales, Universidad de Extremadura, Avda. de Elvas s/n, 06006 Badajoz, España

ARTICLE INFO

Keywords:
Activated carbon
Structured carbon
Carbon black
Electrodes
Supercapacitor
Capacitance
Energy
Power

ABSTRACT

The sharp increase in energy consumption in recent years has increased the demand for new energy storage systems or the improvement of existing ones. Supercapacitors are the answer to this great challenge needed by any industrialized society. In this work, to improve the storage system of these supercapacitors, the composition of carbon-based electrodes has been modified by adding carbon carbonaceous materials and the influence of porous texture (porosity and porosity distribution) on carbonaceous electrodes. Thus, a commercial activated carbon-based electrode PCO-1000 was modified by adding structured carbons TEG, TEG-B92, and carbon black V3. For this purpose, three PCO-1000 (commercial activated carbon) base electrodes were prepared, to which 5 % Teflon was added as a binder and 5 % TEG (structured carbon), TEG-B92 (92 h heat-treated structured carbon) and V3 (carbon black), to provide the electrodes with carbon porous structures, as well as graphitic structures with carbon separation between lamellar layers. The structured carbons (TEG and TEG-B92) have carbon structures formed by interlamellar layers at carbon spacing distances and micro, macroporous pore distributions versus V3 carbon black with meso-macroporous distributions. Furthermore, carbon black V3 was selected as it has a pore distribution (meso-macroporous) greater than 50 Å which is electrochemically accessible by aqueous solutions of H_2SO_4, in an organic medium large solvated ions are not accessible to small pores. The supercapacitor prepared on the PCO-1000 basis with V3 (E-V3), is the best performing, with capacity, power, and energy parameters far superior to the other samples. This seems to indicate that E-V3 supercapacitors with a varied pore structure perform better than those with a predominantly micropore distribution. It seems to be deduced that it is the wide mesopores present in V3 that favour the diffusion of ions inside the carbons.

In conclusion, the resistance of the supercapacitor cell is strongly dependent on the resistance of the electrolyte used, the size of the electrolyte ions in which it diffuses, and the size of the electrode pores, so the characteristics of the electrode material and the electrolyte must be considered together and not separately.

Finally, this study could be of great importance in the fabrication of electrodes with a certain porosity distribution and predominance of wide mesopores and macropores to achieve important energy storage capacities in this type of supercapacitors and their application to hybrid electric vehicles, computers, uninterruptible power supply systems (UPS), motor starters, etc.

1. Introduction

The strong technological increase suffered by humanity in recent years has led directly to an exponential increase in energy demand. The study of new energy storage devices and the achievement of a balance between energy consumption and production is one of the current challenges of society [1,2]. One of these storage devices is supercapacitors (SC). Supercapacitors (SC) consist of two electrodes, a separator, and an electrolyte. The electrolyte is a mixture of positive and negative ions dissolved in water. The two electrodes are separated by a separator. To store as much charge as possible, SCs need to have electrodes with a high surface area to capture many ions at the electrode-electrolyte interface. Generally, the larger the surface area of the electrode, the larger its capacity to accumulate charge. However, this

* Corresponding author.
E-mail address: amacgar@unex.es (A. Macías-García).

https://doi.org/10.1016/j.est.2023.107670
Received 24 February 2023; Received in revised form 10 April 2023; Accepted 7 May 2023
Available online 20 May 2023

surface area must be electrochemically accessible to ions. The availability and wettability of the pores, with dimensions adapted to the size of the solvated cations and anions arriving from the electrolyte, is crucial for good SC performance. The materials for the manufacture of SC electrodes must have a good pore size distribution to ensure a high capacity and a mesopore ratio to facilitate the diffusion of ions and therefore the charge to propagate faster.

Supercapacitors are characterized by storing energy electrostatically on the surface of a material, rather than chemically as in the case of batteries, a considerably long average life, fast response in charge and discharge cycles, and high-power development, although their capacities depend, on a large extent, on the components of their electrodes. One of the most commonly used materials in electrode fabrication are carbon materials [3]. Activated carbon (AC) is an extremely porous form of carbon that has been subjected to an activation process. Activation processes can be thermic or chemical and allow us to control the size and distribution of the pores [4]. The type of material used to obtain activated carbons has a great influence on their adsorbent properties. Lignocellulosic materials (chestnut wood [5], cherry pit [6], walnut [7], kenaf [8], vine shoots [9], holm oak [10]), and materials of industrial origin (used tires [11], etc.) are widely used to obtain activated carbon. Activated carbons are characterized by high internal porosity and high specific surface area. The structure of the carbons has many imperfections, which allows various porous texture possibilities in their preparation [12,13].

Carbon materials are very attractive compounds with great potential to be used as electrodes in supercapacitors due to a combination of physical and chemical properties such as; high conductivity, high specific surface area, good corrosion resistance, high thermal stability, possibility to control their porous texture, easy processability and relatively low cost. Current energy storage systems are very diverse [14], however electrochemical capacitors, generally known as supercapacitors [15] or carbon electrode double layer capacitors (EDLCs), are very attractive devices for portable and automotive systems due to their high specific power and long durability. In most cases, they are used in conjunction with a battery to release high power for a short period of time, which in turn provides high specific power. Some applications of supercapacitors include hybrid electric vehicles, computers, uninterruptible power supplies (UPS), motor starters, etc.

The objective of this work is to study the influence of pore type and pore distribution on the fabrication of carbon electrodes for a supercapacitor.

2. Materials and method

2.1. Raw materials

The following raw materials were used for the manufacture of the supercapacitor electrodes:

2.1.1. Commercial activated carbon, PCO-1000

Commercial activated carbon (PCO-1000) was supplied by Gala. This material has a high specific surface area and high porosity development.

2.1.2. Polytetrafluoroethylene, PTFE

Polytetrafluoroethylene (PTFE) has been used as a binder for electrode fabrication [16].

2.1.3. Carbon black, V3

V3 carbon black was supplied by Cabot Corporation (Spain). The selection of carbon black is based on the results of the study on the electrical conductivity of carbon black under compression published in the journal "Carbon" [17]. Carbon black has been used in the manufacture of electrodes due to its high electrical conductivity.

2.1.4. Structured activated carbon (TEG, TEG-B92)

Graphite has a three-dimensional structure composed of an ordered stacking of graphene planes. The electrical properties of graphitic materials are largely determined by their structure and the bonds between the atoms to form the lattice, which allows the existence of delocalized π electrons, which have high mobility in directions parallel to the plane.

In this work, it is proposed to increase the interlamellar distance between the graphitic layers by heat treatment, in order to improve their physicochemical properties, in terms of electrical conductivity, intercalation capacity, etc. [18]. Thus, the samples of structured activated carbons obtained are modifications of the graphitic layers, carried out in the laboratory, to improve some of their properties.

The structured activated carbons were prepared by heat treatment of TEG expanded graphite and heat treatment of TEG for 92 h (TEG-B92). The objective of this type of treatment is to obtain a graphitic structure with larger interlaminar distances than the original graphite.

2.2. Textural characterization of the carbons

The characterization of the porous structure of the carbon samples was carried out using N_2 adsorption isotherms at 77 K (−196 °C) and Horvath-Kawazoe (HK) method [19,20], DFT (Density Functional Theory) [21] and BJH (Barrett-Joyner-Halenda) model [22].

The HK method [19,20]allows to obtain a distribution of the porosity of the solid in the micropore zones from the region of low relative pressures of the adsorption isotherm.

The DFT [21] allows studying the pore size distribution in the narrow micropore and mesopore zone.

The BJH [23] method allows the calculation of the thickness of the adsorbed layer and the mean pore radius.

2.3. Supercapacitors

For the study of the supercapacitors, Swagelok type electrochemical cells were used, and the measurements were performed on a Metrohm Autolab PGSTAT101 potentiostat-galvanostat.

Commercial activated carbon (PCO-1000), vulcanized carbon black (V3), two types of structured activated carbon (TEG and TEG-B92), and PTFE diluted in water at 60 % by weight as a binder material were used to fabricate the electrodes, which are 7 mm in diameter.

The components of each electrode, as well as their proportions, are shown in Table 1.

Considering the results obtained by other researchers and by us in other works, it was decided to use an aqueous electrolyte, H_2SO_4 0.5 M prepared in the laboratory [24] separator element.

2.3.1. Electrochemical characterization

To study the behaviour of the designed supercapacitors, they have been subjected to cyclic voltammetry tests and galvanostatic charge-discharge processes.

2.3.1.1. Cyclic voltammetry. Cyclic voltammetry is a technique based on the application of an electrical potential perturbation in the form of a linear variation as a function of time and recording the response current [25]. For this work, cyclic voltammetry has been carried out using

Table 1
Electrode composition.

	E-TEG	E-TEG-B92	E-V3
PCO-1000(%)	**85**	**85**	**85**
PTFE (%)	**10**	**10**	**10**
TEG (%)	**5**	0	0
TEG-B92 (%)	0	**5**	0
V3 (%)	0	0	**5**

The numbers in bold indicate the percentage composition of the electrode.

sweep speeds of between 0.005 and 0.05 V/s.

These experiments are intended to calculate carbon parameters of the active material of the electrode, such as the specific capacitance, the charge accumulated during the cathodic and anodic sweeps (Q_c and Q_a), the coulombic efficiency (μ), which is the quotient between these two values.

The capacitance of an electrode (C) in farads (F) is determined by the expression (2.1). [26,27].

$$C(F) = \frac{\int_{E_0}^{E_f} IdV}{s\Delta V} \tag{2.1}$$

where ΔV is the potential window in which you are working. To obtain the specific capacitance, divide with C by the grams of electrode material.

The coulombic efficiency μ is calculated according to the expression (2.2):

$$\mu(\%) = \frac{Q_c}{Q_a} \times 100 \tag{2.2}$$

2.3.1.2. Galvanostatic charge-discharge. Galvanostatic charge-discharge is the measurement of the potential of a system as a function of time while a constant current is applied [25]. By obtaining the potential versus time curves, it is possible to calculate the capacitance of the supercapacitor (C), the equivalent series resistance of the system (ESR), as well as the maximum energies and powers of the system (E_{max} and P_{max} respectively). Thus, expression (2.3) allows the calculation of the capacitance of the device:

$$C_{device} = \frac{I(A)}{slope_{discharge}(Vs^{-1})m_{mt}} \times 100 \tag{2.3}$$

The ERS is calculated by dividing the ohmic drop at the start of the discharge (ΔV) by the change in current in the supercapacitor as given in Eq. (2.4):

$$ERS\left(\Omega \cdot cm^2\right) = \frac{\Delta V}{2 \cdot I} A \tag{2.4}$$

The maximum energy is calculated by Eq. (2.5):

$$E_{maximum} = \frac{1}{2} CV^2 \tag{2.5}$$

Finally, by means of expression (2.6), it is possible to obtain the maximum power:

$$P_{maximum} = \frac{V^2}{4ESR} \tag{2.6}$$

3. Results and discussion

In this section, the characterization and study of a commercial activated carbon, two structured carbons, and a carbon black are described and discussed. Subsequently, the application of these activated carbons as electrodes for supercapacitors is analyzed.

3.1. Characterization of the carbonaceous materials

The results obtained from the characterization of the four carbons are described and discussed below:

3.1.1. Textural characterization

The porous texture of the starting materials in the micropore and narrow mesopore region was determined from adsorption isotherms, and the porosity in the wide mesopore and macropore region was analyzed by mercury porosimetry.

The N_2 adsorption isotherms at −196 °C obtained for the samples are shown in Fig. 1.

Fig. 1 shows that the PCO-1000 sample presents a type I isotherm, typical of microporous solids, with pore size less than a few times the diameter of the adsorbate molecule. At small values of relative pressure (p/p_0), a closed bend is observed, typical of the presence of micropores and where the adsorption process practically takes place in this type of pore. Also, for higher values of relative pressure, a "plateau" appears in the isotherm, indicating that the pores are filled by the adsorbate [28].

On the other hand, the TEG, TEG-B92, and V3 samples show type III isotherms, typical of non-porous adsorbents or those containing large

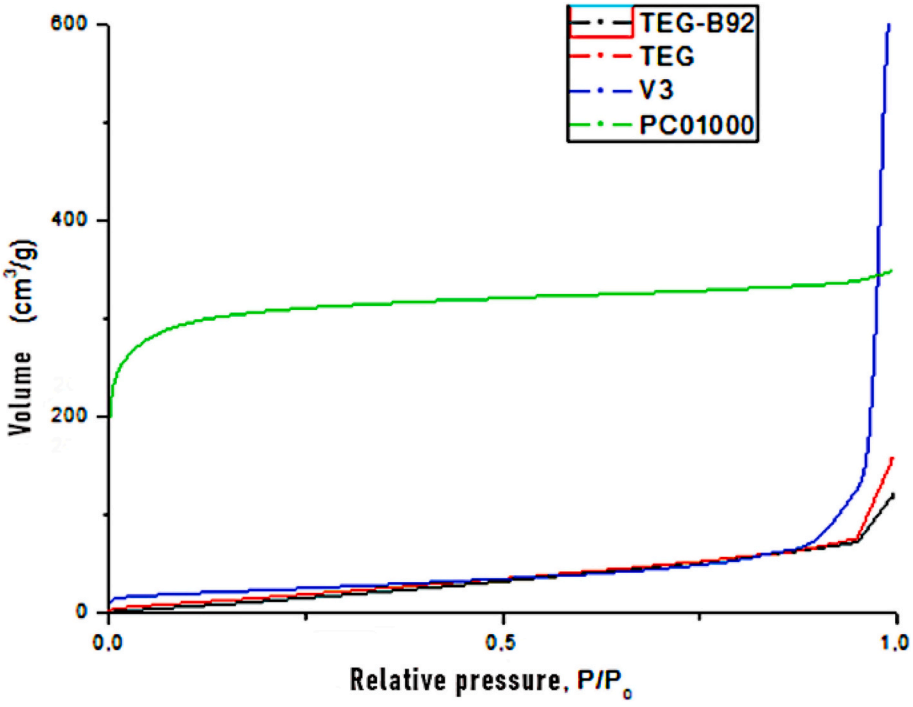

Fig. 1. N_2(g) adsorption isotherms at −196 °C from carbons.

pores (macropores). The inflection point, or knee point, of the isotherm denotes that the first layer, or monolayer, of adsorbate on the adsorbent surface has been completed. At higher p/p_0 values, multilayer adsorption continues, forming the second and subsequent layers. When saturation is reached, the number of layers is infinite [28].

As can be seen in Fig. 1, the sample PCO-1000 shows a higher porous development of micropores and narrow mesopores than the rest of the samples. The remaining samples show a lower pore development in general, with predominance of macropores.

In order to corroborate the above analysis, the textural parameters listed in Table 2 have been determined.

The S_{BET} of the samples follow the following order PCO-1000 > TEG-B92 > V3 > TEG.

The S_{BET} of the samples follows the following order PCO-1000 > TEG-B92 > V3 > TEG. Sample PCO-1000 shows higher S_{BET} and porosity values than other activated carbons of narrow micro-mesoporous lignocellulosic origin [29].

The Table shows the carbon porosity distributions of the samples, it can be observed that PCO-1000 presents mainly narrow micropores-mesopores, TEG macropores, TEG-B92 less quantity of macropores and V3 wide mesopores-macropores, which makes these samples adequate to study their influence in the fabrication of electrodes for supercapacitors.

To study these aspects further, the pore size distribution in the micropore and narrow mesopore zones was studied using the DFT method. The results of this study are shown in Fig. 2.

As can be seen in Fig. 2, the most significant pore development occurs, for all the samples, in the micropore zone (0–20 Å). This graph shows that the commercial activated carbon PCO-1000 has a very pronounced distribution of micropores compared to the other samples. On the other hand, the remaining samples have very similar micropore distributions.

To establish the difference in pore size corresponding to the other samples, it has been studied by means of the graphical representation shown below (Fig. 3):

As can be seen in Fig. 3, the pore size distribution in the range from 0 to 160 Å has been graphically represented in order to analyze more clearly the pore size in both the micropore and narrow mesopore ranges. In the range of micropores 0 to 20 Å, and narrow mesopores 20 to 160 Å, it is observed that samples TEG, TEG-B92, and V3 present a very similar pore size distribution. Comparing these three samples, a higher pore development is observed for a pore width of 16 Å, which is repeated in the samples.

In order to complete the porous study, it is of great interest to know the porosity in the mesopore-wide and macropore zones. To this end, the data obtained by mercury porosimetry have been studied, as shown in Figs. 4 and 5.

Fig. 4 plots the cumulative volume versus pressure, showing steep slopes in the low-pressure range indicating the filling of larger pores (TEG and V3) and a very large "plateau" over a wide pressure range, suggesting that the samples have little or no wide mesoporous structure (TEG-B92 and PCO-1000).

From the mercury porosimetry data shown in Fig. 5, the values corresponding to the volumes of mesopores and macropores in Table 2 were obtained, from which it can be seen that the TEG and TEG-B92 samples lack the development of wide mesopores, presenting a marked macroporous character, which seems to indicate the existence of

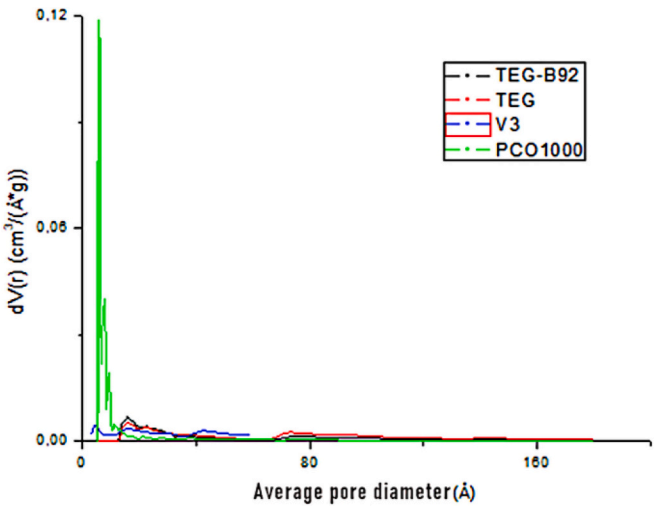

Fig. 2. Pore size distribution representation for carbons (DFT method).

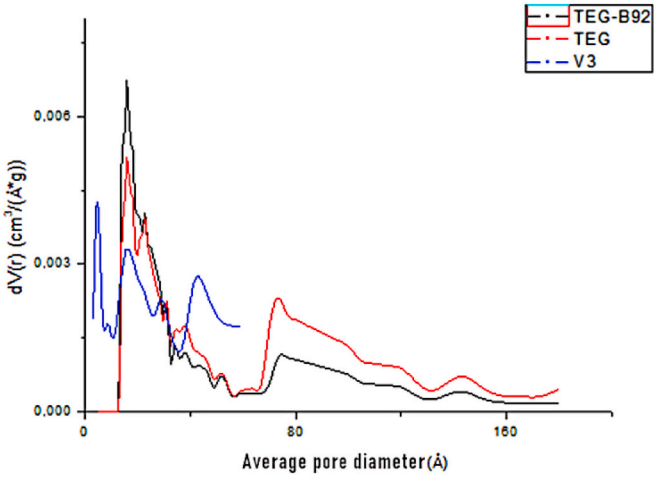

Fig. 3. Study of pore development in the range (0–160 Å).

a separation between the layers, as corresponds to structured activated carbons, which give rise to a high macroporous development [30]. On the other hand, samples PCO-1000 show a meso-macroporous porous development, being much more pronounced as expected in sample V3, typical of carbon black.

On the other hand, Fig. 6 shows the most interesting zone for the samples of the structured carbon TEG and TEG-B92, as well as for sample V3, where a significant pore development can be seen, corresponding to the macropore zone for sample TEG.

These very carbon behaviours will allow us to study the influence that electrodes with this type of pore distribution have on supercapacitors [31].

3.2. Supercapacitors

From the carbons, a series of supercapacitors have been prepared,

Table 2
Textural data of the samples studied.

Samples	S_{BET} ($m^2 \cdot g^{-1}$)	V_{mi} ($cm^3 \cdot g^{-1}$)	V_{me} ($cm^3 \cdot g^{-1}$)	$V_{me\text{-}p}$ ($cm^3 \cdot g^{-1}$)	$V_{ma\text{-}p}$ ($cm^3 \cdot g^{-1}$)	V_T ($cm^3 \cdot g^{-1}$)
PCO-1000	1178	0,444	0,502	0,075	0,187	1405
TEG	71	0,015	0,100	0	1,75	1865
TEG-B92	83	0,009	0,098	0	0,224	0,331
V3	80	0,030	0,114	0,62	0,74	0,1504

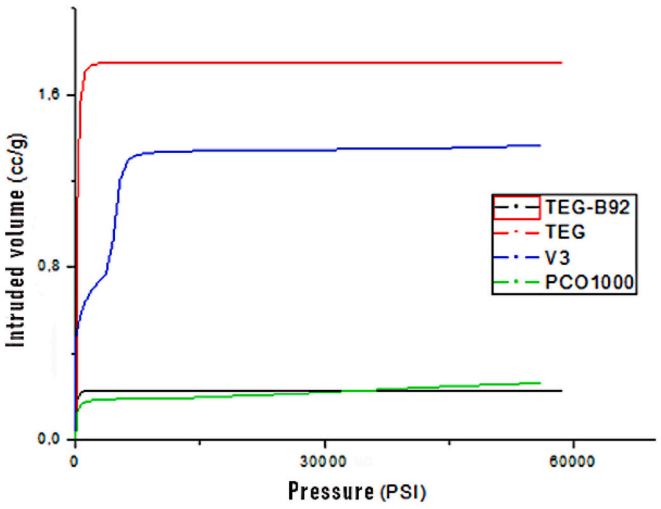

Fig. 4. Intruded volume versus pressure, for carbon carbon samples.

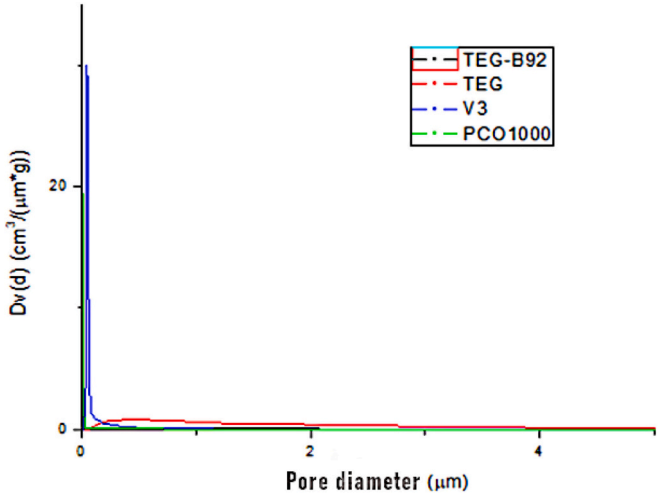

Fig. 5. Cumulative volume versus pore diameter of carbons.

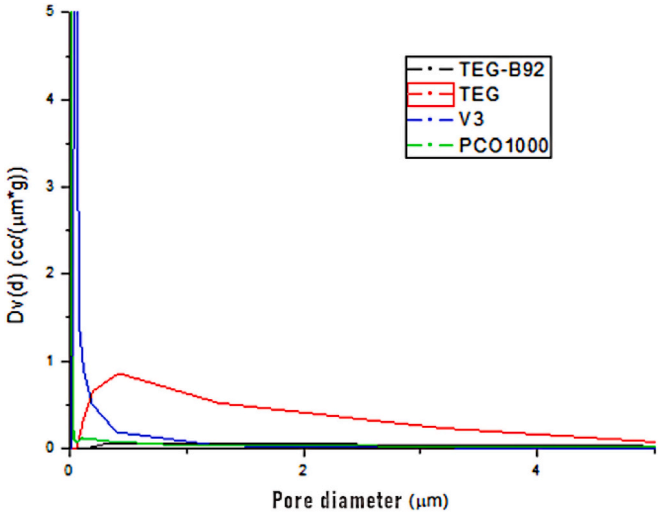

Fig. 6. Detail of Fig. 5.

consisting of commercial activated carbons and binding agents (PVDF), and another one with the addition of V3, TEG, and TEG-92. The objective was to improve a commercial activated carbon PCO-1000 by adding carbon-structured carbons TEG and TEG-B92 and compare them with traditional electrodes used in supercapacitors to which V3 carbon black are added to improve their electrical conductivity [32,33]. At the same time, this study allows the influence of pore size to be studied, given the disparity in the pore volume of the samples [31].

The electrodes that are part of the supercapacitors are referenced in Table 1 and the resulting supercapacitors are named E-TEG, E-TEG-B92, and E-V3 because these materials are the differential component between them.

3.2.1. *Electrochemical characterization*

The electrodes (E) were prepared from the materials and proportions listed in Table 1. To determine the electrical properties of the supercapacitors, the samples were subjected to cyclic voltammetry and galvanostatic charge-discharge techniques, which provide information both on the capacity to store energy and on properties such as maximum power and energy that can be supplied.

3.2.1.1. Cyclic voltammetry. The parameters established for the experiment are shown in Tables 3–5, using 1 V as the potential window, delimited by the potential that the electrolyte used can withstand. The maximum current intensity range used is the maximum supported by the 1 mA measuring equipment. Each sample was subjected to six cycles in which the scanning speed was varied. Figs. 7–9 show the voltammograms of the carbon samples.

Fig. 7 shows the voltagram of the E-TEG sample in H_2SO_4 0,5 M at carbon scanning speeds. As the sample E-TEG has a heterogeneous porous structure with carbon pore sizes and a contribution of 5 % TEG (macroporous carbon) compared to 85 % PCO-1000 (micro-mesoporous carbon, with a predominance of narrow mesopores close to the micropores), a limitation in the diffusion of ions into the pores, typical of microporous carbons, can be observed at high scanning speeds. This phenomenon results in an apparent increase in resistance at high sweep speeds.

The sample E-TEG shows good coulombic efficiency, as there is no large deviation between the charge accumulated in the anodic and cathodic region, as shown in Table 3 and evident in Fig. 7. The capacitance values are higher for low sweep speeds.

Fig. 8 shows the voltagram of the E-TEG-B92 sample in H_2SO_4 0,5 M at carbon scanning speeds. As it is a sample with a less porous structure than the previous one and equally heterogeneous with carbon pore sizes and with a contribution of 5 % of TEG-B92 (low porous carbon), compared to 85 % of PCO-1000 (micro-mesoporous carbon), with a predominance of narrow mesopores close to the micropores, a limitation in the diffusion of ions towards the pores is more pronounced than in the E-TEG sample at the carbon scanning speeds, which results in a smaller cycle area and lower specific capacities.

The sample shows a good coulombic efficiency, as there is no large deviation between the charge accumulated in the anodic and cathodic region, as shown in Table 4 and evident in Fig. 8. The capacitance values are higher for low sweep speeds.

Table 3
Cyclic voltammetric properties of the E-TEG sample.

Mass (g)	Potential window (V)	Cycle	Sweep speed (V/S)	Cycle area	Specific capacity (F/g)	Coulombic efficiency µ(%)
0,0234	1	1	0,005	0,15287	30,57412	47,73857
		2	0,01	0,25563	25,56322	80,34566
		3	0,02	0,40132	20,06596	90,71794
		4	0,03	0,46987	15,66235	92,58713
		5	0,04	0,50641	12,66032	92,98485
		6	0,05	0,50474	10,0947	93,42889

Table 4
Cyclic voltammetric properties of sample E-TEG-B92.

Mass (g)	Potential window (V)	Cycle	Sweep speed (V/S)	Cycle area	Specific capacity (F/g)	Coulombic efficiency μ(%)
0,0346	1	1	0,005	0,13805	27,61002	51,97333
		2	0,01	0,23084	23,08423	84,31912
		3	0,02	0,33939	16,96963	93,49186
		4	0,03	0,38809	12,93647	93,92151
		5	0,04	0,40365	10,09128	93,60933
		6	0,05	0,40143	802857	93,57374

Table 5
Cyclic voltammetric properties of sample E-V3.

Mass (g)	Potential window (V)	Cycle	Sweep speed (V/S)	Cycle area	Specific capacity (F/g)	Coulombic efficiency μ(%)
0,0214	1	1	0,005	0,21052	42,10593	37,18,441
		2	0,01	0,35789	37,78916	72,58367
		3	0,02	0,53946	26,97277	88,67819
		4	0,03	0,62044	20,68128	91,40795
		5	0,04	0,64138	16,03476	92,13457
		6	0,05	0,63303	12,66062	92,37676

Fig. 9 shows the voltagram of sample E-V3 in H_2SO_4 0,5 M at carbon scanning speeds. As it is a sample with a more heterogeneous structure, in general, than the previous ones and with a contribution of 5 % of V3 (wide meso-macroporous carbon), compared to 85 % of PCO-1000 (narrow micro-mesoporous carbon, with a predominance of narrow mesopores close to the micropores), a better diffusion of the ions towards the pores than in the previous samples can be seen at the carbon scanning speeds, which gives rise to a greater cycle area and higher specific capacities [34].

The sample shows good coulombic efficiency, as there is no large deviation between the charge accumulated in the anodic and cathodic region, as shown in Table 5, and clearly seen in Fig. 9. The capacitance values are higher for low sweep speeds and higher with respect to the other samples.

3.2.1.2. Galvanostatic charge-discharge. Figs. 10–12 show the graphs corresponding to the galvanostatic charge-discharge. These graphs consider the potential jump, through which the equivalent series resistance of the supercapacitor can be calculated, and the slope of the discharge part, which provides information to calculate the capacitance of the supercapacitor and the other characteristic parameters.

From Fig. 10, the charging stage shows an ascending line of almost constant slope (first section), where the maximum potential is reached. In the second (descending) section, a potential drop of 0.2 V is observed. The discharge stage is determined by the downward leg with a slope of 0.0123. Knowing these data, the parameters listed in Table 6 can be calculated, which have been calculated according to the expressions (2.3)–(2.6) described above [35].

Fig. 11 corresponds to sample E-TEG-B92. The loading and unloading stages are similar to Fig. 10, because this sample was prepared from the previous one by means of thermal treatment. The figure shows an ascending line with an almost constant slope where the maximum

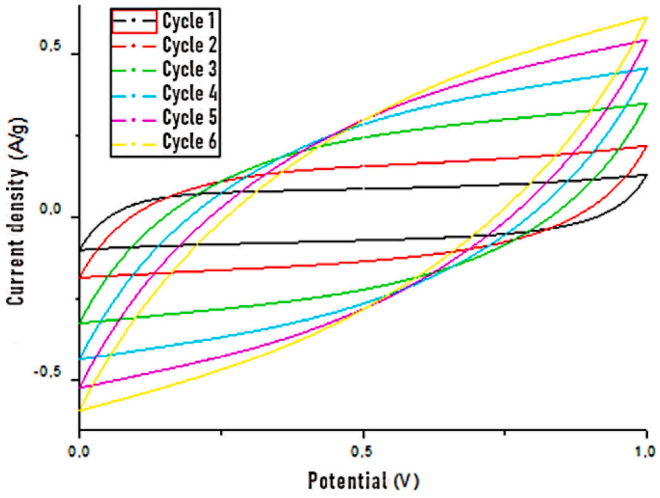

Fig. 8. Cyclic voltammetry of sample E-TEG-B92.

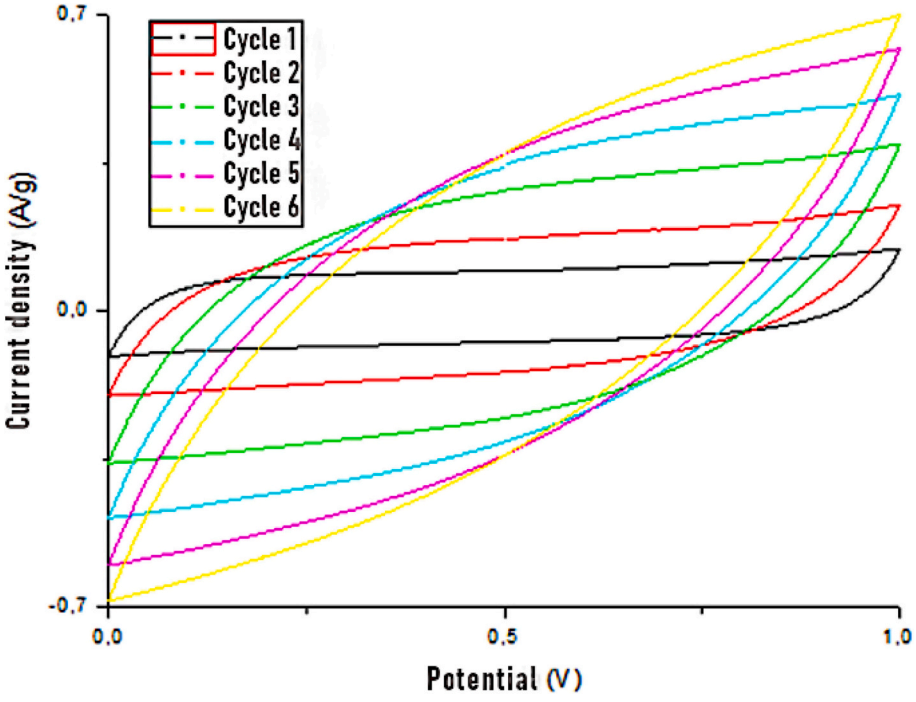

Fig. 7. Cyclic voltammetry of the sample E-TEG.

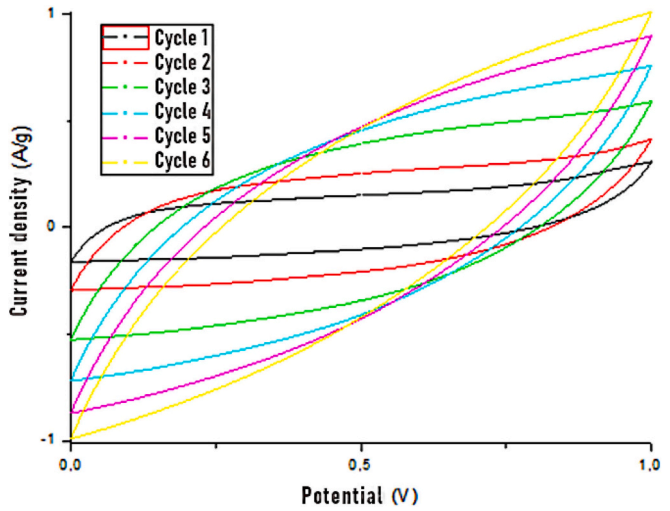

Fig. 9. Cyclic voltammetry of sample E-V3.

potential is reached and a descending section with a potential drop of 0.13 V, which is smaller than the previous one. The discharge stage is determined by the descending section with a slope of 0.0086.

If we compare these results with the previous sample, we can say that in the second (descending) section the potential drop is slightly lower than in the previous case, as well as the slope of the discharge stage. This implies a lower value of the equivalent series resistance (ESR) of the device, which causes it to provide very similar capacitance values, as would be expected given the origin of the two samples.

In view of Fig. 12 corresponding to sample E-V3, two well carboniated behaviours can be observed in the ascending section, the first one practically linear until reaching potential values above 0.8 V, after which a steep curve is produced until reaching the maximum potential.

In the descending section, the potential drop is an intermediate 0.17 V than in the previous samples.

The discharge slopes of sample E-V3 have the same value as sample E-TEG-B92.

As previously observed, the supercapacitor prepared with V3, carbon black presents higher energy, power, and capacity values than the previous ones, which shows that although the structured carbons TEG and TEG-B92 improve the performance of the commercial carbon, it is the carbon black V3 which gives quantitatively better results. Furthermore, depending on the electrolyte medium, carbon black V3 was selected as it has a pore distribution (meso-macroporous) greater than 50 Å which is electrochemically accessible by aqueous solutions, in an organic medium large solvated ions are not accessible to small pores.

In conclusion, the resistance of the supercapacitor cell is strongly dependent on the resistance of the electrolyte used, the size of the electrolyte ions in which it diffuses and the size of the electrode pores, so the characteristics of the electrode material and the electrolyte must be considered together and not separately.

4. Conclusions

Carbon carbons have been studied: activated carbon, structured carbons, and carbon black, from a textural point of view. Depending on the results, carbon electrodes have been prepared to analyze their influence on their application in a supercapacitor. In view of the results, it can be concluded that:

a) Textural characterization showed that the carbon used as the basis for preparing the PCO-1000 electrodes had a porous texture developed micro-mesoporous, compared to the other carbons in which a predominance of mesopores (V3) or macropores (TEG and TEG-92) was observed.
b) In view of the above results, three PCO-1000 base electrodes were prepared, to which were added 5 % Teflon as a binder and 5 % TEG, TEG-B92, and V3, (carbon pore distributions) and carbon types of graphitic structures with larger interlaminar distances than graphite (TEG and TEG-92).
c) The E-TEG and E-TEG-B92 structured carbons provided very carbon textural parameters, mainly macropores for the supercapacitor, which was totally related, on the one hand, to the treatments undergone by both samples. Thus, the supercapacitor formed by E-TEG electrodes presents higher capacity than E-TEG-B92 probably due to

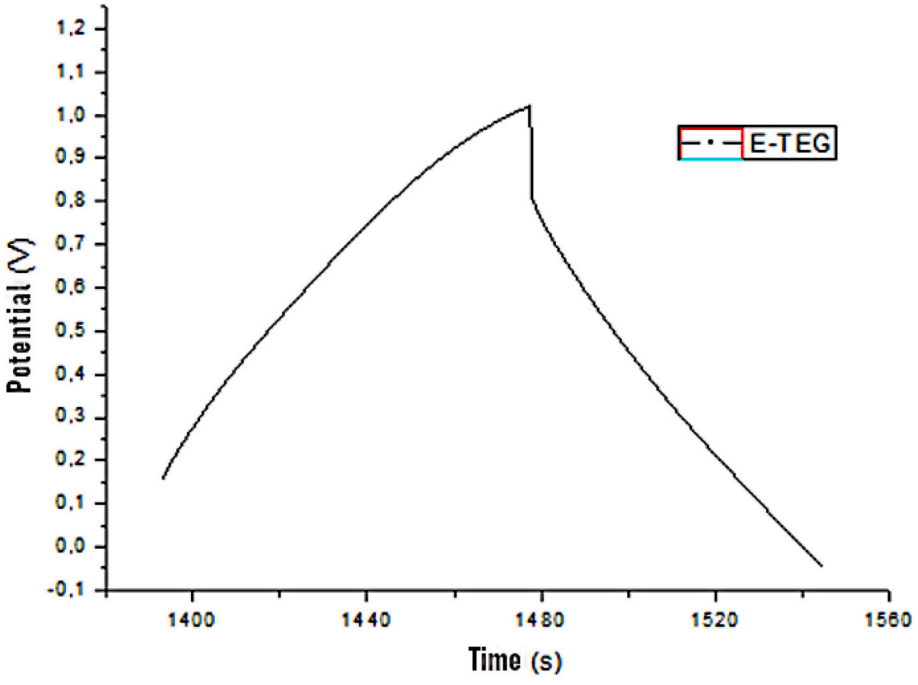

Fig. 10. Galvanostatic charge-discharge of the sample E-TEG.

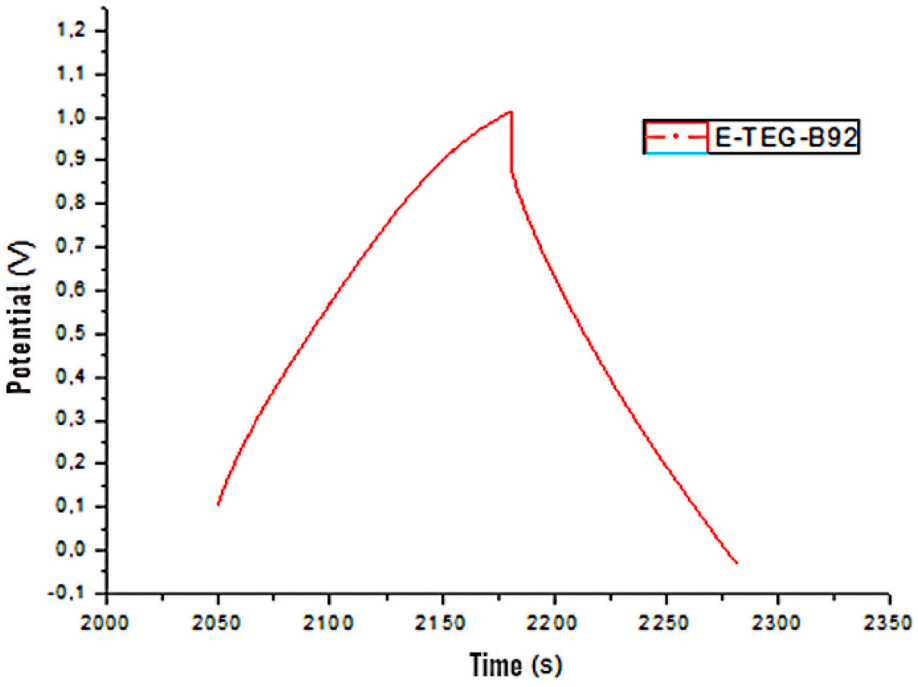

Fig. 11. Galvanostatic charge-discharge of sample E-TEG-B92.

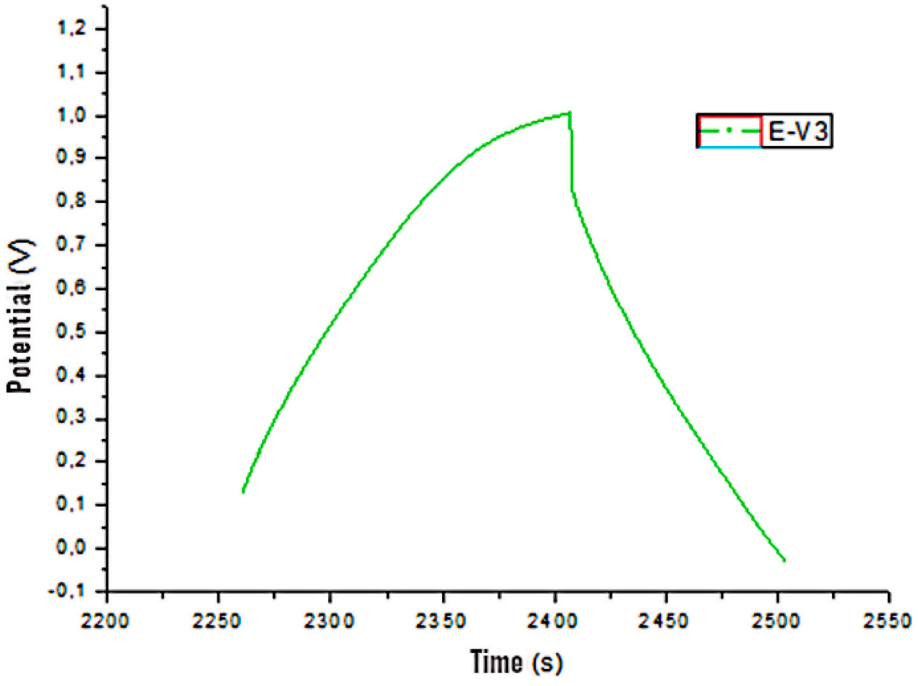

Fig. 12. Galvanostatic charge-discharge of sample E-V3.

Table 6
Galvanostatic charge and discharge properties for the samples.

	Potential drop (V)	I (A)	Mass (g)	Discharge slope	Cell (F/g)	ESR ($\Omega \cdot cm^2$)	E_{max} (Wh/kg)	P_{max} (kW/kg)	C_{total} (F/g)
E-TEG	0,2155	0,005	0,0234	−0,0123	17,372	79,632	34,7439	0,0314	69,488
E-TEG-B92	0,1339	0,005	0,0346	−0,0086	16,803	49,516	33,6067	0,0505	67,213
E-V3	0,1712	0,005	0,0214	−0,0086	27,168	63,277	54,3360	0,0395	108,67

a mainly macroporous structure more developed which favours the diffusion of ions.

d) The supercapacitor prepared based on PCO-1000 with V3 (E-V3) showed the best results, with capacity, power, and energy parameters much higher than the rest of the samples. This seems to indicate that supercapacitors with a more heterogeneous pore structure, with a predominance of wide mesopores and macropores, perform better than those with a smaller and less heterogeneous pore distribution, probably because this type of distribution facilitates ion diffusion.

e) Finally, in view of the carbon types of pores and their influence on the behaviour of the E-V3 supercapacitor, it seems to be deduced that it is the mesopores that favour the diffusion of ions inside the carbons, which would lead to a better behaviour of the supercapacitor, in our case the E-V3 supercapacitor.

CRediT authorship contribution statement

Jesús M. Rodríguez-Rego: Investigation and software.
Laura Mendoza-Cerezo: Investigation, Review & Editing.
Alfonso C. Marcos-Romero: Supervision and software.
Juan P. Carrasco-Amador: Supervision and validation.
A. Macías-García: Writing - Original Draft and conceptualization.

Declaration of competing interest

The authors declare that they have no known competing financial interests or personal relationships that could have appeared to influence the work reported in this paper.

Data availability

Data will be made available on request.

References

[1] J. Zhang, J. Gai, K. Song, W. Chen, Advances in electrode/electrolyte interphase for sodium-ion batteries from half cells to full cells, Cell Rep. Phys. Sci. 3 (5) (May 2022) 100868, https://doi.org/10.1016/J.XCRP.2022.100868.

[2] J. Ge, L. Fan, A.M. Rao, J. Zhou, B. Lu, Surface-substituted Prussian blue analogue cathode for sustainable potassium-ion batteries, Nat. Sustain. 5 (3) (Mar. 2022) 225–234, https://doi.org/10.1038/S41893-021-00810-7.

[3] S. Vaquero Morata, Diseño y caracterización de supercondensadores de alta energía basados en materiales carbonosos, Universidad Autónoma de Madrid, Madrid, 2015. Accessed: Apr. 06, 2023. [Online]. Available: https://repositorio.uam.es/handle/10486/666387.

[4] D. Qu, Studies of the activated carbons used in double-layer supercapacitors, J. Power Sources 109 (2) (Jul. 2002) 403–411, https://doi.org/10.1016/S0378-7753(02)00108-8.

[5] V. Gómez-Serrano, E.M. Cuerda-Correa, M.C. Fernández-González, M.F. Alexandre-Franco, A. Macías-García, Preparation of activated carbons from chestnut wood by phosphoric acid-chemical activation. Study of microporosity and fractal dimension, Mater. Lett. 59 (7) (Mar. 2005) 846–853, https://doi.org/10.1016/J.MATLET.2004.10.064.

[6] M. Olivares-Marín, C. Fernández-González, A. Macías-García, V. Gómez-Serrano, Preparation of activated carbon from cherry stones by chemical activation with ZnCl2, Appl. Surf. Sci. 252 (17) (Jun. 2006) 5967–5971, https://doi.org/10.1016/J.APSUSC.2005.11.008.

[7] V. Gómez-Serrano, E.M. Cuerda-Correa, M. Carmen Fernández-González, M. F. Alexandre-Franco, A. Macías-García, Preparation of activated carbons from walnut wood: a study of microporosity and fractal dimension, Smart Mater. Struct. 14 (2) (Feb. 2005) 363, https://doi.org/10.1088/0964-1726/14/2/010.

[8] E.M. Cuerda-Correa, A. Macías-García, M.A.D. Díez, A.L. Ortiz, Textural and morphological study of activated carbon fibers prepared from kenaf, Microporous Mesoporous Mater. 111 (1) (Apr. 2008) 523–529, https://doi.org/10.1016/J.MICROMESO.2007.08.025.

[9] B. Corcho-Corral, M. Olivares-Marín, C. Fernández-González, V. Gómez-Serrano, A. Macías-García, Preparation and textural characterisation of activated carbon from vine shoots (*Vitis vinifera*) by H_3PO_4—chemical activation, Appl. Surf. Sci. 252 (17) (Jun. 2006) 5961–5966, https://doi.org/10.1016/J.APSUSC.2005.11.007.

[10] A. Macias-García, M.J. Bernalte García, M.A. Díaz-Díez, A. Hernández Jiménez, Preparation of active carbons from a commercial holm-oak charcoal: study of micro- and meso-porosity, Wood Sci. Technol. 37 (5) (Mar. 2004) 385–394, https://doi.org/10.1007/S00226-003-0191-7.

[11] E. Manchón-Vizuete, A. Macías-García, A. Nadal Gisbert, C. Fernández-González, V. Gómez-Serrano, Preparation of mesoporous and macroporous materials from rubber of tyre wastes, Microporous Mesoporous Mater. 67 (1) (Jan. 2004) 35–41, https://doi.org/10.1016/J.MICROMESO.2003.10.002.

[12] F. Rodríguez-Reinoso, Microporous structure of activated carbons as revealed by adsorptive methods, Chem. Phys. Carbon 21 (1) (Jan. 1988) 141. Accessed: Apr. 06, 2023. [Online]. Available: https://www.researchgate.net/publication/312912452_Microporous_structure_of_activated_carbons_as_revealed_by_adsorptive_methods.

[13] B. McEnaney, Properties of activated carbons, in: F. Schüth, K.S.W. Sing, J. Weitkamp (Eds.), Handbook of Porous Solids, John Wiley & Sons, Ltd, Bath, 2008, pp. 1828–1863, https://doi.org/10.1002/9783527618286.CH24B.

[14] B.K. Kim, S. Sy, A. Yu, J. Zhang, Electrochemical supercapacitors for energy storage and conversion, in: Handbook of Clean Energy Systems, John Wiley & Sons, Ltd, 2015, pp. 1–25, https://doi.org/10.1002/9781118991978.HCES112.

[15] Y. Gogotsi, Carbon Nanomaterials 2nd ed., vol. 1, CRC/Taylor & Francis, 2006. Accessed: Apr. 06, 2023. [Online]. Available: https://books.google.com/books/about/Carbon_Nanomaterials.html?hl=es&id=RM9knQ2_4nIC. Accessed: Apr. 06, 2023. [Online]. Available:.

[16] S. Ebnesajjad, Expanded PTFE applications handbook: technology, manufacturing and applications, in: S. Ebnesajjad (Ed.), Expanded PTFE Applications Handbook: Technology, Manufacturing and Applications, 1st ed., Elsevier Inc., 2016, pp. 1–286.

[17] J. Sánchez-González, A. Macías-García, M.F. Alexandre-Franco, V. Gómez-Serrano, Electrical conductivity of carbon blacks under compression, Carbon N Y 43 (4) (Jan. 2005) 741–747, https://doi.org/10.1016/J.CARBON.2004.10.045.

[18] P. Solís Fernández, Modificación superficial de materiales de carbono: grafito y grafeno, Universidad de Oviedo, Oviedo, 2011. Accessed: Apr. 06, 2023. [Online]. Available: https://digital.csic.es/bitstream/10261/34323/1/TESIS-Pablo%20Solis.pdf.

[19] G. Horváth, K. Kawazoe, Method for the calculation of effective pore size distribution in molecular sieve carbon, J. Chem. Eng. Japan 16 (6) (Dec. 1983) 470–475, https://doi.org/10.1252/JCEJ.16.470.

[20] G. Horvath, Energetic interactions in phase and molecular level pore characterisation in nano-range, Colloids Surf. A Physicochem. Eng. Asp. 141 (3) (Nov. 1998) 295–304, https://doi.org/10.1016/S0927-7757(97)00191-X.

[21] R. Evans, U. Marini Bettolo Marconi, P. Tarazona, Fluids in narrow pores: adsorption, capillary condensation, and critical points, J. Chem. Phys. 84 (4) (Aug. 1998) 2376, https://doi.org/10.1063/1.450352.

[22] M. Polovina, B. Babić, B. Kaluderović, A. Dekanski, Surface characterization of oxidized activated carbon cloth, Carbon N Y 35 (8) (Jan. 1997) 1047–1052, https://doi.org/10.1016/S0008-6223(97)00057-2.

[23] M. Polovina, B. Babić, B. Kaluderović, A. Dekanski, Surface characterization of oxidized activated carbon cloth, Carbon N Y 35 (8) (1997) 1047–1052, https://doi.org/10.1016/S0008-6223(97)00057-2.

[24] A. Macías-García, D. Torrejón-Martín, M.Á. Díaz-Díez, J.P. Carrasco-Amador, Study of the influence of particle size of activate carbon for the manufacture of electrodes for supercapacitors, J. Energy Storage 25 (1) (Oct. 2019) 100829, https://doi.org/10.1016/J.EST.2019.100829.

[25] A.J. Bard, L.R. Faulkner, Electrochemical Methods: Fundamentals and Applications, 2nd ed., Wiley, 2001.

[26] S. Vaquero Morata, Diseño y caracterización de supercondensadores de alta energía basados en materiales carbonosos, Universidad Autónoma de Madrid, Madrid, 2015. Accessed: Dec. 26, 2022. [Online]. Available: https://repositorio.uam.es/handle/10486/666387.

[27] B.K. Kim, S. Sy, A. Yu, J. Zhang, Electrochemical supercapacitors for energy storage and conversion, in: Handbook of Clean Energy Systems, 2015, pp. 1–25, https://doi.org/10.1002/9781118991978.hces112.

[28] J.M. Martín Martínez, Adsorción física de gases y vapores por carbones, in: Adsorción Física de Gases y Vapores por Carbones, 1990, pp. 312–400. Accessed: Apr. 06, 2023. [Online]. Available: https://dialnet.unirioja.es/servlet/libro?codigo=176286&info=resumen&idioma=SPA. Accessed: Apr. 06, 2023. [Online]. Available:.

[29] F. C. C., A. T. D., R. G. C., Surface area of activated and modified charcoals obtained from agricultural resources *Saccharum officinarum*, Rev. Cienc. Agríc. 34 (2) (Dec. 2017) 62–72, https://doi.org/10.22267/RCIA.173402.72.

[30] H. Lu, et al., Understanding the effects of electrode meso-macropore structure and solvent polarity on electric double layer capacitors based on a continuum model, Chin. J. Chem. Eng. 50 (Oct. 2022) 423–434, https://doi.org/10.1016/J.CJCHE.2022.06.011.

[31] X. Zhang, et al., Porous and graphitic structure optimization of biomass-based carbon materials from 0D to 3D for supercapacitors: a review, Chem. Eng. J. 460 (Mar. 2023), 141607, https://doi.org/10.1016/J.CEJ.2023.141607.

[32] C.A. Frysz, D.D.L. Chung, Improving the electrochemical behavior of carbon black and carbon filaments by oxidation, Carbon N Y 35 (8) (1997) 1111–1127. Accessed: Dec. 26, 2022. [Online]. Available: https://www.academia.edu/79760532/Improving_the_electrochemical_behavior_of_carbon_black_and_carbon_filaments_by_oxidation. Accessed: Dec. 26, 2022. [Online]. Available:.

[33] C.A. Frysz, X. Shui, D.D.L. Chung, Electrochemical behavior of porous carbons, Carbon N Y 35 (7) (1997) 893–916, https://doi.org/10.1016/S0008-6223(97)00039-0.

[34] A.B. Fuertes, F. Pico, J.M. Rojo, Influence of pore structure on electric double-layer capacitance of template mesoporous carbons, J. Power Sources 133 (2) (Jun. 2004) 329–336, https://doi.org/10.1016/J.JPOWSOUR.2004.02.013.

[35] B.E. Conway, W.G. Pell, Power limitations of supercapacitor operation associated with resistance and capacitance distribution in porous electrode devices, J. Power Sources 105 (2) (Mar. 2002) 169–181, https://doi.org/10.1016/S0378-7753(01)00936-3.